

# Application of Edge and Line Detection to Detect the near Surface Anomalies in Potential Data

Lenka Kosková Trísková and Josef Novák

*The Institute of Novel Technologies and Applied Informatics, Technical University in Liberec, Studentská 2,  
Liberec, Czech Republic*

Keywords: Edge Detection, Field Anomaly Detection, Potential Field Data, Gravity.

Abstract: Presented paper is focused on fast near surface anomaly detection in potential data. Our aim is to find fast and semi-automated anomaly detection technique for the near surface anomalies with defined geometry. The proposed algorithm is based on the shape recognition. The edge and line detection is used on acquired data to detect the typical shape of the anomaly. Shape geometry parameters are converted into the anomaly parameters and location information. The technique was tested using a set of noise-free and noisy synthetic gravity data; satisfactory results were obtained.

## 1 INTRODUCTION

The general idea of presented algorithm is to speed up the initial search processes after an event such as flooding or earthquake with the geophysical methodology. We face a set of limitations: time, hardware, power and network accessibility is limited. The operation itself runs in unstable and dangerous circumstances. Finally – after the disaster, no fully qualified geophysical specialist is available on site. Any semi-automated data pre-processing is very useful in such situation.

In described application, there is no interest in the detailed 3D model of the subsurface materials. The main interest is in local anomalies with typical characteristics, such as cavities in dams.

Desired algorithm should be able to answer questions: What is a probability of presence of a significant anomaly with defined density and geometry in the current data? If it is present, where is it located?

According to the application constraints, we are interested to detect the anomalies near the surface – the depth fits into the range from 0 to 50 m. The highest detection accuracy is expected in the depth interval from 0 to 20 m. Typical search pattern is an object with contrast density (a cavity filled by air or water), contrast resistivity (the buried infrastructural networks).

The initial methodology testing was made using analytical data for the spherical and cylindrical

gravity anomaly (in both vertical and horizontal position).

The desired anomaly forms typical shapes in the acquired data. Anomaly with sphere-like geometry gives circle contours in data, wires, pipes and similar geometries lead to lines in data.

Due to application constraints we are looking for the fast and simple process. The presented application is therefore based on smoothing (Shih, 2010), morphological processing (Shih, 2010), shape detection and finally anomaly classification. The algorithm works well for all tested geometries.

For future enhancement and more complex anomaly geometry, we plan to use CNN support for the shape classification (Aydogan, 2012; Li et al., 2011) or textural analysis (Cooper, 2004).

All the presented algorithms were implemented and tested in the Matlab software.

## 2 THEORY AND METHODS

### 2.1 The Anomaly

A general function presenting a symmetric potential field anomaly can be expressed by simple equation (Salem, 2011):

$$f(r) = \frac{F}{(r^2 + z^2)^q} \quad (1)$$

$F$  is an amplitude factor,  $q$  is a shape factor characterizing the shape of the anomaly. The  $r$  is the

distance from the middle point of the anomaly to the observation point on the surface. Detailed summary of  $q$  and  $F$  values for different simple geometrical bodies both for gravity and magnetic sources is given for example in Salem (2011); in short it is presented in Table 1. More complex anomaly geometry can be derived from theory presented in the Blakely (pages 192-213).

Table 1: The  $F$  and  $q$  factor for simple geometrical bodies, gravity field ( $\gamma$  is gravitational constant,  $M$  is mass for the sphere and density contrast times cross-sectional area for the cylinder).

| Anomaly type        | $F$          | $q$   |
|---------------------|--------------|-------|
| Sphere              | $\gamma Mz$  | $3/2$ |
| Horizontal cylinder | $2\gamma Mz$ | $1$   |
| Vertical cylinder   | $\gamma M$   | $0.5$ |

Considering simple anomaly bodies, the  $f$  function is a smooth function; maximum value is located above the anomaly center. If the anomaly field is presented as 2D image, it gives spherical contours for sphere and vertical cylinder, for horizontal cylinder we obtain linear contours.

For all three bodies a linear dependency between the depth of anomaly center ( $z$ ) and the surface location of the half-maximum value ( $x_{0.5}$ ):

$$z = k \cdot x_{0.5} \tag{2}$$

The  $k$  value differs with anomaly type and its value can be extracted directly from the equation (1) (Mares, 1990; pages 55-57). The  $z$  value can be later used to estimate the density (or mass) of the anomaly directly from the equation (1).

Table 2: The value of the  $k$  parameter for different anomaly types.

| Anomaly type        | $K$                  |
|---------------------|----------------------|
| Sphere              | $1.305$              |
| Horizontal cylinder | $1$                  |
| Vertical cylinder   | $\frac{\sqrt{3}}{3}$ |

## 2.2 The Detection Process

The detection process itself contains following steps (all the steps are described deeply later in the text):

1. The noise level enhancement based on histogram analysis (optional).
2. Smoothing, if noise is detected (optional).
3. The detection of areas with value close to maximum and half maximum.
4. Conversion of the maximum and half maximum matrices into black and white pictures.

5. Line detection in maximum matrix – a line significant for horizontal cylinder. The detection of sphere and vertical cylinder is started otherwise.
6. Shape detection in half maximum matrix to measure the appropriate  $x_{0.5}$  value using the maximum and half maximum matrix.
7. The parameters estimation and calculation of estimated anomaly field. If no lines detected in the image, both spherical and cylindrical fields are calculated and compared with original image – the closest shape is selected.

## 2.3 Noise and Smoothing

The noise in general can have a lot of sources (from measurement errors to the noise of the measurement equipment or the influence of the deeper anomalies). In our application, the noise is simulated as a white noise with selected level, which is added to the original analytical data.

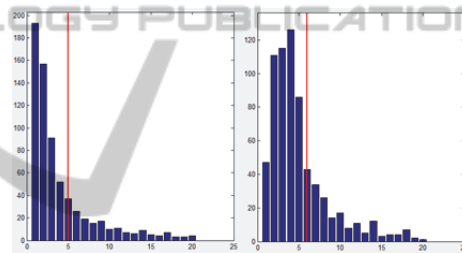


Figure 1: The histogram of a noise free spherical anomaly (left picture) and noisy spherical anomaly (right picture, noise level is from 0 to 0.2 of the maximum value).

All analytical data have very typical histogram, which is depicted in Figure 1 on the left. The biggest set of data has value close to the minimum. The mean value is also closer to the minimum. The peak at the minimum value is typical for higher mass and small depth. (For the horizontal cylinder, most of the values are less than a mean value of data.) White noise has all values equally distributed between the minimum and maximum value; the mean value is in the middle of the maximum and minimum. By general, each desired anomaly has its typical histogram shape which can be tested on input data. The histogram itself is not a key to determine the anomaly shape. It can help to detect the noise and to separate “nonsense” data without any searched anomaly shape.

If a noise is detected the smooth filter is used. The 3x3 and 5x5 averaging and Gauss smoothing kernels were applied (Shih, 2010; page 52), best results were obtained with averaging 3x3 filter. If

the histogram shows high noise level in the data, the smoothing is repeated from 2 to 3 times.

### 2.4 Shape Detection

In the next step the maximum and half maximum matrix is created: All the values higher than 98 % of the maximum are colored in white, other left black in the maximum matrix (MM). All the values higher than 50 % of the maximum are white in the half maximum matrix (HM).

Line detection process is now necessary to distinguish the horizontal cylinder and other anomalies – it is necessary to set up the thresholds of following erosion process. We use the standard Hough transform according to the Matlab (2009).

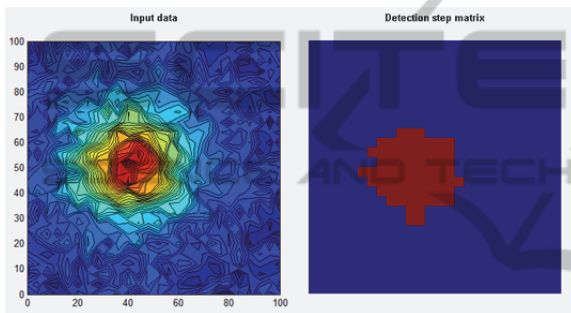


Figure 2: The spherical anomaly with noise (left picture, noise level is from 0 to 0.2 of the maximum value) and corresponding MM matrix.

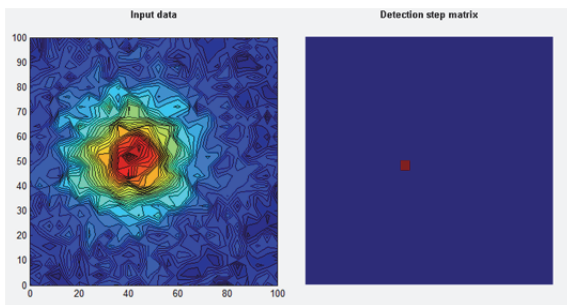


Figure 3: The spherical anomaly with noise (left picture, noise level is from 0 to 0.2 of the maximum value) and corresponding MM matrix after erosion.

Next step is the erosion of the MM matrix, as the erosion pattern is used the Golay alphabet, the L element (Golay, 1969). The aim of the erosion is thin the white areas (for a pixel or a single line). This way we get the location of the middle of the anomaly.

Now the HM matrix is taken into the account. If lines were detected, we run the line detection again, to get the border of the half value area (half middle

line). The distance between the middle line and half middle line is calculated using standard algebra algorithms for the line distance measurements.

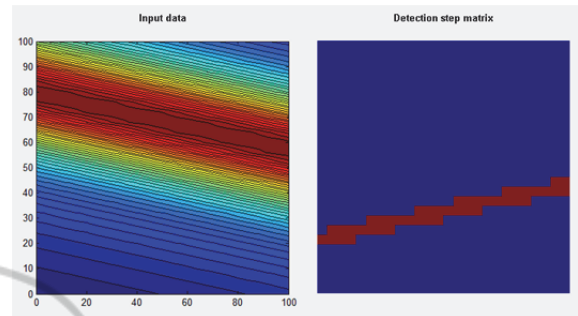


Figure 4: The horizontal cylinder without noise (left picture) and corresponding MM matrix after erosion.

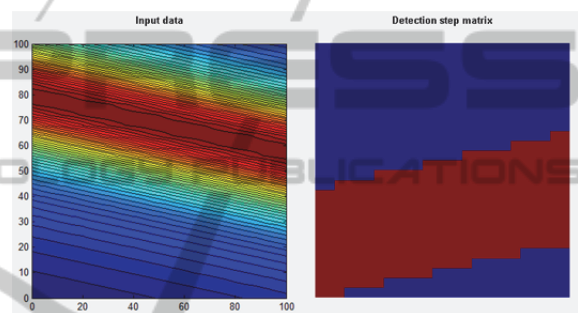


Figure 5: The horizontal cylinder without noise (left picture) and corresponding HM matrix.

If no line is detected, we estimate the width and height of the white area in HM matrix. If the shape is not close to the circle, the process ends with result “no desired anomaly is detected”. Otherwise, the distance from the middle point to the border of the half maximum circle is measured.

Measured distance is in the next step used to estimate the density or mass of the anomaly.

The estimated parameters are used with equation (1) to calculate the estimated anomaly field. If the horizontal cylinder was already detected in the data (the initial line detection was successful), the process ends.

If no lines were detected, it is now necessary to distinguish the sphere and vertical cylinder. The euclidean distance between the input ( $f_i$ ) and estimated ( $f_e$ ) field is measured point by point for both estimated anomaly fields and input data:

$$R(f_i, f_e) = \sqrt{|f_i^2 - f_e^2|} \tag{3}$$

The result is the distance matrix. The mean value of this matrix is taken as the error number  $ErrNum$ , the description of the similarity of input and estimated field. The less is the  $ErrNum$ , the closest are values

in the input and estimated field. The estimated shape of the anomaly is selected as the shape of the estimated data with lower ErrNum.

### 3 CONCLUSIONS

The presented shape detection algorithm detects the analytical anomaly body in both noise-free and noise data. If low level noise is presented in the data, the algorithm works well without smoothing the data; higher level of noise in the data requires the smoothing.

The spherical anomaly detection with high level of added noise is presented in Figure 6, horizontal cylinder with the same level of noise in Figure 7, vertical cylinder is presented in Figure 8. In all figures, the data area is 100x100 m with 4 m step.

In general, the estimation error differs from 80 % to 99 % in the depth and location estimation. The geometry is detected correctly in 80 %. The most of the failures is obtained with high noise and horizontal cylinder. For the future we plan to enhance the shape detection of HM matrix to obtain the more precise detection and to improve the comparison of the similarity of the estimated and input data.

The real application of presented algorithm requires to define the desired anomaly body and to modify the proper way the shape detection steps.

If no desired anomaly is presented in data, we can see it in histogram and also during the shape detection process (the HM matrix has different than expected characteristics).

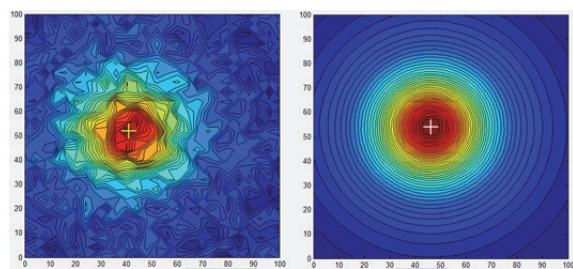


Figure 6: The spherical anomaly with noise (left picture, noise level is from 0 to 0.2 of the maximum value) and estimated value. Original depth is 23 m, estimated is 25 m.

### REFERENCES

Aydogan, D., 2012, *CNNEDGE POT: CNN based edge detection of 2D near surface potential field data*, Computers & Geosciences, vol. 46, p. 1-8.

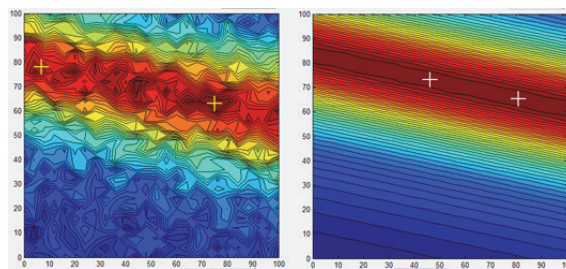


Figure 7: The horizontal cylinder with noise (left picture, noise level is from 0 to 0.2 of the maximum value) and estimated value. Original depth is 22 m, estimated is 23 m.

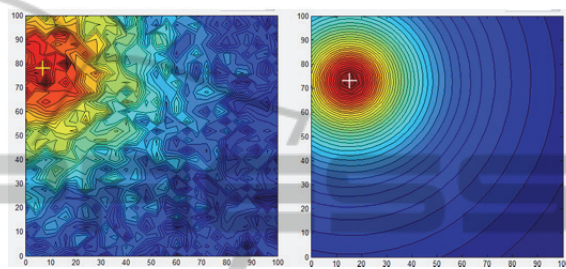


Figure 8: The vertical cylinder with noise (left picture, noise level is from 0 to 0.2 of the maximum value) and estimated value. Original depth is 22 m, estimated is 16 m.

- Cooper, G. R. J., 2004, *The textural analysis of gravity data using co-occurrence matrices*, Computers & Geosciences, vol. 30, p. 107-115.
- Blakely J. R., 1995, *Potential Theory in Gravity & Magnetic Applications*, Cambridge University Press. Cambridge.
- Golay, M. J. E., 1969, *Hexagonal Parallel Pattern Transformations*, IEEE Transactions on Computers, vol. 8, p. 733 – 740.
- Li H., Liao X., Li C. et al., 2011, *Edge detection of noisy images based on cellular neural networks*, Communications in Nonlinear Science and Numerical Simulation, vol. 16, p. 3746-3759.
- Mareš S., 1990. *Úvod do užité geofyziky*, SNTL. Praha, 2<sup>nd</sup> edition.
- Matlab, 2009, *Image processing toolbox manual*, Mathworks.
- Salem A., 2011. *Multi-deconvolution analysis of potential field data*, Journal of Applied Geophysics, vol. 74, p. 151-156.
- Shih F. Y., 2010. *Image processing and pattern recognition – Fundamentals and Techniques*, John Wiley and Sons. New York.